Journal of Oceanography, Vol. 65, pp. 803 to 816, 2009

Different Spreading of Somali and Arabian Coastal Upwelled Waters in the Northern Indian Ocean: A Case Study

VINU VALSALA*

Center for Global Environmental Research, National Institute for Environmental Studies, Tsukuba 305-8506, Japan

(Received 15 January 2009; in revised form 19 July 2009; accepted 19 July 2009)

The spreading pathways of the Somali and Arabian coastal upwelled waters in the northern Indian Ocean are identified from an ocean re-analysis data set of a single year using numerical passive tracers in a transport model. The Somali and Arabian coastal upwelled waters are found to have entirely different spreading pathways in the northern Indian ocean. The former circulates anticyclonically, is mixed vertically, and is advected to the eastern Indian Ocean along the north equatorial region; while the later intrudes into the northern Arabian Sea, circulates anticyclonically and is advected to the south in the central Arabian Sea and then to the eastern Indian Ocean. The seasonal surface mixing by strong monsoon winds and sheared currents due to dominant eddies of the Somali region are found responsible for mixing 25% of Somali upwelled water with the subsurface and affecting the resultant pathways. The effect of mixing is, however, found negligible in the case of Arabian coastal upwelled water pathways. The seasonal reversal of circulation and eddy dominance during the southwest monsoon cause the Somali upwelled water to spread over the northern Indian Ocean faster than the simultaneously upwelled Arabian coastal water.

Keywords:
· Somali coast,
· Arabian coast,
· Arabian Sea,
· upwelling,
· trajectory,
· pathways,
· SODA,
· tracers,
· offline model,
· Indian Ocean.

1. Introduction

The pathways of upwelled water from the western coastal Arabian Sea in the northern Indian Ocean are examined using a numerical ocean model. The Indian Ocean experiences seasonally reversing monsoon wind systems that result in seasonally altering circulations in the upper ocean and different upwelling and downwelling zones. In contrast to other world oceans, the winds over the northern equatorial Indian Ocean are westerlies during the boreal (northern) summer. These westerlies, combined with the trade winds in the south, cause a net Ekman transport from the northern Indian Ocean to the southern Indian Ocean connected by a shallow equatorial roll at the equator (Miyama *et al*., 2003). In order to compensate this surface southward Ekman transport, water subducts in the southern Indian ocean and circulates to the north along the thermocline, is routed through the western boundary currents, and upwells at various coastal and open ocean regions in the northern Indian Ocean. Among these upwelling zones, the most significant ones appear along the Somali coast and the coast of Arabia, which includes the coast of Yemen and Oman. This shallow meridional circulation in the Indian Ocean (confined above 500 m) is known as the cross-equatorial circulation (Schott *et al*., 2002; Miyama *et al*., 2003).

The main upwelling zone in the northern Indian Ocean is situated in the western Arabian Sea coast, mainly along the Somali coast (Schott *et al*., 1990, 1997; Schott and McCreary, 2001). The observations suggest that 4 to 7 Sv of water is upwelled along the Somali coast on average (Schott *et al*., 2002). The upwelling is phase-locked with the southwest monsoon winds. The Somali upwelling commences during the onset of the southwest monsoon (from late May), peaks during July, August and September and decays to a downwelling at the arrival of the northeast monsoon. Apart from the Somali region, the other sites of upwelling zones are along the Arabian coast (coast of Oman and coast of Yemen). The Arabian coast upwelling is about 1.2 to 4.5 Sv on average (Schott *et al*., 2002).

A few studies had discussed the surface pathways of the upwelled water in the northern Indian Ocean in connection with its cross-equatorial transport to the south (e.g. Miyama *et al*., 2003; Jensen, 2003). However, none of

* E-mail address: vinu.valsala@nies.go.jp

these studies had addressed a detailed structure of the surface pathways of the upwelled water in the northern Indian Ocean. More specifically, the relative importance of each of the upwelling zones of the Arabian Sea on the total coastal upwelling and the individual pathways of the water that upwelled from each of the upwelling zones are unknown. This is an important theme to investigate because the upwelling causes the nutrient-rich subsurface water to surface (Sharada *et al*., 2008). The supply of nutrients may vary from one upwelling zone to the other according to the nutrient availability in the subsurface water and the strength of upwelling. Consequently, the spatial and temporal spreading of nutrients from each upwelling zone may differ largely. This may have a potential impact on the spatial variability of the regional biogeochemistry system in the western Arabian Sea. In this study, we will examine more specific pathways of the upwelled water from each of the coastal upwelling zones of the western Arabian Sea.

The role of the western Arabian Sea coastal upwelling in the Indian monsoon rainfall has been studied in an analysis that combines observations and coupled model experiments (Izumo *et al*., 2008). The study points out that a decrease in upwelling does strengthen the monsoon rainfall along the west coast of India by increasing the Sea Surface Temperature (SST hereafter) along the Somali-Oman coasts. Montegut *et al*. (2007) showed that the eastern and western Arabian Sea have distinct mixed layer heat budgets and pointed out that the penetration of solar heat flux needs to be taken into account in these two subbasins. The upwelling water surfaces nutrient-rich subsurface water, and subsequent chlorophyll availability may have a potential impact on masking solar insolation in the mixed layer (Wiggert *et al*., 2006). Therefore, the pathways of upwelling waters are worth analyzing. Montegut *et al*. (2007) also suggested that, in the western Arabian Sea, the vertical processes as well as the horizontal advection contribute significantly to the SST interannual variability.

Although the return pathways of the upwelling water to the southern Indian Ocean are well explained through the southward Ekman transport estimations, the surface spreading and the horizontal structure of the southward flow are not well identified yet. Some studies have raised this concern partially. For example, Jensen (2003) has investigated the cross-equatorial transport of tracers and salt from the northern Indian Ocean to the south and their return pathway to the north through the western boundary currents. In an excellent attempt by combining the results of an Ocean General Circulation Model (OGCM), a 1.5-layer model and a linear continuously-stratified model, Miyama *et al*. (2003) examined the pathways of the cross-equatorial cell in the Indian Ocean and identified the meridional structure of this circulation in detail. In a recent study, using Lagrangian particles and passive tracers in an OGCM, Valsala and Ikeda (2007) have also investigated the major three-dimensional spreading pathways in the Indian Ocean. However, their study focused only on the pathways of Indonesian throughflow (ITF) water.

The returning of the upwelling water to the southern Indian Ocean via Ekman transport has significant impact on the Indian Ocean climate because of its net southward heat transport. To date, an accurate estimate of this southward heat transport of the Indian Ocean is not available. The World Ocean Circulation Observations suggest a net southward heat transport of 1.5 PW to south of 30°S (Ganachaud and Wunsch, 2000), which may include transport from the Indonesian Throughflow as well as a contribution from the significant heat flux in the southern tropical Indian Ocean. A more relevant net southward heat transport across 5°S is reviewed in Godfrey *et al*. (2007); table 1; and it ranges from 0.57 to 1.1 PW in observations and 0.11 to 0.60 PW in models. Taking advantage of Argo floats, new estimates are becoming available.

Owing to the seasonally-reversing circulation in the northern Indian Ocean, the upwelled water in the Arabian Sea is expected to show dramatic seasonality in its pathways. In this study, the spreading pathways of the upwelled water from two upwelling sites are considered separately. The two sites of interest here are the Somali coast and the Arabian coast (this includes the coasts of Yemen and Oman). The Somali upwelling is at its peak during July–August. The strong western boundary currents accompanying with this upwelling reach as high as 2 ms^{-1} (Schott *et al*., 1997).

To answer the following questions is the goal of this study: (1) What are the pathways of the upwelled water from the different western coasts of Arabian Sea? (2) What is the time scale associated with the spreading of the upwelled water from each upwelling zone? Section 2 introduces the model and experiments used in this study. The pathways of water from two upwelling zones are investigated in Section 3. The results and uncertainties are discussed in Section 4 followed by a summary in Section 5.

2. The Data, Model, and Experiments

2.1 Ocean data

This study makes use of the Simple Ocean Data Assimilation (SODA.2.0.2) re-analysis ocean currents prepared by Carton and Giese (2008). The SODA is an ocean reanalysis product widely used to evaluate the upper ocean climate change in the past five decades. This data set is made from the Parallel Ocean Program (POP) configuration of the Modular Ocean Model (MOM) with a sequential update of approximately 7×10^6 observational pro-

files of temperature and salinity from the World Ocean Database (Conkright *et al*., 2001) and the US National Oceanic and Atmospheric Administration/National Oceanic Data Center archives. In addition to the historic and time-series observations of temperature and salinity, the observations from a number of Argo profiles since early 2000 are also incorporated into the SODA system. More details of the model configuration and design can be found in Carton and Giese (2008).

The original SODA.2.0.2 is simulated at a horizontal resolution of $0.25° \times 0.4°$, which may be sufficient to resolve the meso-scale features. In this study the SODA.2.0.2 with a resolution of $0.5° \times 0.5° \times 40$ levels is used. Among the 40 vertical levels the first 20 levels are above the depth of 579 m.

In this article we have used the SODA data prepared for the year 2000 as a case study for investigating the pathways of the Arabian Sea upwelled water. The choice of this year for our experiment is mainly because we are interested only in the mean pathways of the Arabian Sea coastal upwelled water in the northern Indian Ocean and any interannual variability in these pathways is not a subject of interest in this study. The year 2000 is assumed here as a scenario closer to the climatology (Krishnan *et al*., 2000), but will serve for the general purpose of the present study. The order of uncertainty that may arise out of this assumption is addressed in Subsection 4.1.

2.2 Tracer transport model

In order to find the pathways of the Arabian Sea upwelled water, we have employed a novel strategy of passive tracer transport modeling using the SODA reanalysis ocean currents. The tracer transport modeling method of Valsala *et al*. (2008) is adopted here. In this method an OGCM circulation, temperature, salinity and other diagnostic physical parameters are used in an offline-mode to evolve an advection-diffusion passive tracer. The offline tracer transport model is optimized for SODA.2.0.2 data set and is used in this study. The parameters we obtain from the SODA data are the 2D-circulation, temperature, salinity, mixed layer depth, freshwater flux, net surface heat flux and sea surface height. The vertical velocities are found by the mass conservation principles. The surface boundary exchanges fresh water with the atmosphere via evaporation and precipitation, which appear as velocities on the top cell face of the model surface grid. The free-surface kinematic boundary condition is provided from the sea surface height. The seasonal surface vertical mixing is parameterized through KPP scheme as in Large *et al*. (1994) since the mixing coefficients are not readily available from the SODA data, and is calculated within the model using the circulation and water properties. In addition to a Laplacian horizontal diffusion that we provide for the computational stability, an isopycnal diffusion of Redi (1982) type and eddy induced transport of Gent and McWilliams (1990) type are also incorporated into the offline model.

In the work of Valsala *et al*. (2008), the tracer transport model was extensively tested with the simulation of Chlorofluorocarbon-11 (CFC). For this test the offline circulations and other physical parameters were derived from the GFDL (Geophysical Fluid Dynamics Laboratory, Princeton) reanalysis data products. However, in the present study we have optimized the same model for SODA.2.0.2 circulations because of its wide usage and higher resolution. The transport model optimized for SODA data is tested for mass conservation and CFC-11 simulations. The limitations in simulating the tropical mixing are also eliminated in the newer version of the offline model.

The offline data are provided as monthly means since sub-monthly outputs are not available, and are interpolated into a model time step of two hours for the tracer simulations. A monthly offline input feeding may attenuate the high frequency variability under 30 days in the pathways. Since large scale spreading pathways are seasonally driven (Jensen, 2003) they are likely to be represented in the present model setup as well. In a separate experiment using a fine resolution (~25 km) 2.5-layer reduced-gravity online model forced with daily scatterometer winds, we found that the large scale pathways were closely similar except for the differences attributed to the vertical mixing, which is not resolved in the reduced gravity model. In the high-resolution simulation, however, mesoscale filaments were more pronounced. Therefore, the pathways derived here may have attenuated filaments compared to the real ocean. The results here are considered consistent qualitatively with the monthly inputs although quantitative differences may be expected.

2.3 Experiments

The tracer is introduced into the model domain from the Somali and Arabian coast in separate experiments. The tracer is injected whenever a vertical velocity on the bottom face of the uppermost model tracer cell along the coast is found positive. In order to represent the total coastal upwelling, the tracer is injected not only at the exact coast but also at any grid within 250 km off the coast. The upwelling in the Somali coast is not only driven by the local wind stress but also by the non-linear interaction of strong western boundary currents with the coastal topography. The Somali upwelling is found to be stronger along the coast and in the northern flanks of the Great Whirl (GW) and Socotra Eddy (SE) (Schott *et al*., 1997). The tracer is injected at a unit number per unit volume of water. The concentration is directly proportional to the vertical velocity of the upwelling.

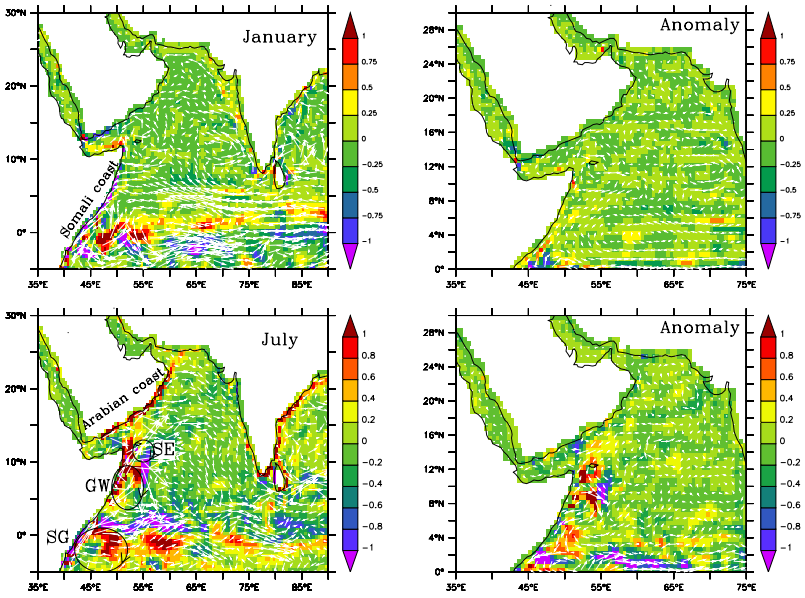

Fig. 1. Arabian Sea circulation as derived in SODA.2.0.2 for the year 2000. The vertical velocity at the bottom of the first level of the data is indicated by shading (positive values indicate upward velocities) and the surface currents in the first level of the data are shown as vectors for January and July. Vertical velocity and vectors are given in $\times 10^{-5}$ ms^{-1} and ms^{-1}, respectively.

All the experiments are run for a total of five years starting from January with repeating monthly circulations from the SODA data of the year 2000. The tracers representing the Somali and Arabian coast upwelled water are referred to as Somali Tracer (ST), Arabian Tracer (AT), respectively.

2.4 Arabian Sea circulation

Figure 1 shows the surface 3D-circulation for January (upper left panel) and July (lower left panel) in the year 2000. The major features of the model circulations resemble the observed general circulation of the north Indian Ocean. During the northeast monsoon (normally spans from December to February) the North Equatorial Current (NEC) is found as a broad current from the equator to 7°N whose core intensifies as it reaches the western Indian Ocean (Schott and McCreary, 2001). Just south of the equator to 7°S is the Equatorial Counter Current (ECC), which is the most intense current in the western part of the basin during the winter monsoon. The NEC and ECC have alternating northward and southward meridional currents, which are most obvious near the western boundary. They were previously identified as the presence of high-frequency waves in the equatorial waveguide such as Mixed Rossby-Gravity (MRG) waves with a westward phase velocity and an eastward group velocity (Sengupta *et al.*, 2004). Kindle and Thompson (1989) have found that 30 to 40-day oscillations in the equatorial Indian Ocean are also associated with the instability waves.

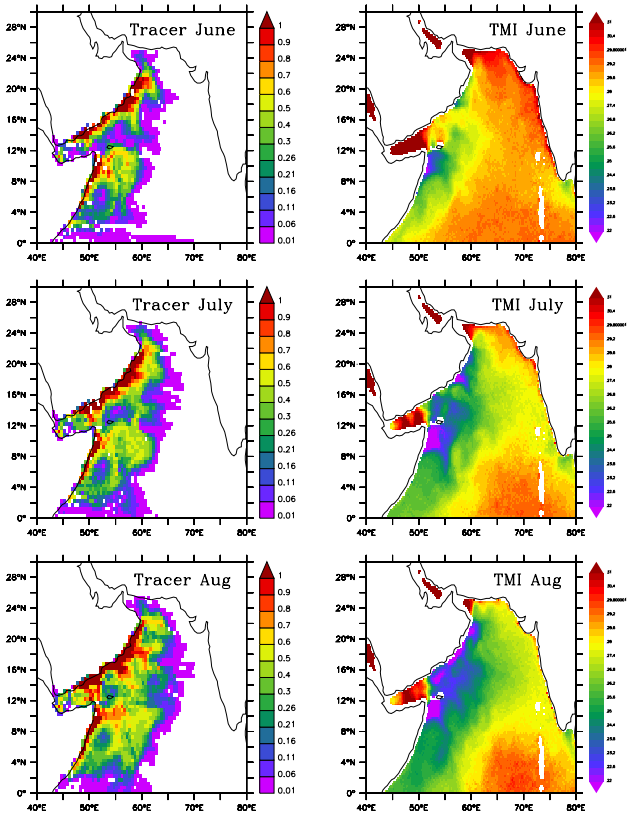

Fig. 2. The sum of Somali and Arabian coastal tracers for the months between June and August in the first year at the surface level of the model (left panel). The TMI SST (°C) during the period is shown in the right panel. The tracer unit is per unit volume.

During the southwest monsoon, the NEC reverses its direction and flows to the west as the summer monsoon current (SMC hereafter). The strongest current of the basin is the cross-equatorial transport of Somali current that reaches an average transport of 29 Sv during the summer monsoon. The cross-equatorial flow is southward in the interior ocean due to the net southward Ekman transport connected with shallow overturning circulations at the equator (Miyama *et al.*, 2003). During the southwest monsoon, the dominance of GW, Southern Gear (SG), and SE are visible in the circulation field and they are in agreement with the observations of Schott *et al*. (1997) and Schott and McCreary (2001).

Throughout the year, the Arabian coast has numerous eddies propagating westward along the coast. These are mainly generated due to the non-linear interaction between the currents and the coastal boundary friction (Jensen, 1991). The elimination of non-linear terms in a 1.5-layer model by Shankar and Shetye (1997) has indicated that the majority of these eddies were removed from the solution. The major eddies that form during the southwest monsoon season are GW and SE. The formation of GW is due to the barotropic instability (i.e. strong horizontal shear) of the surface currents, while SE and other surrounding eddies are maintained by the baroclinic supply of energy (Jensen, 1991). During the onset of southwesterly winds (i.e. from the month of May onwards), GW starts to mature and a strong upwelling along the coast as well as along the northern flank of GW starts to appear. The water properties show a cold water filament flanking the northern part of GW and along the Somali coast where deep cold water surfaces by upwelling. The maximum current along the coast exceeds a speed of 2 ms^{-1} (Schott *et al*., 1997).

We compared the evolution of surface elevations in the SODA data with the TOPEX/POSEIDON altimetry data (figure not shown). It was observed that SODA and TOPEX/POSEIDON sea surface height anomalies were well correlated. The prominent eddies were simulated at the exact locations and periods as found in the observations, especially during the formation and maturing phases. For instance, SODA GW and SE showed evolutions comparable to the observations. Moreover, SG, which is another prominent circulation feature in the western boundary of the Indian Ocean, was also well simulated in the model. These eddies may have significant roles in determining the pathways of the upwelled water masses across the surface Indian Ocean (Weller *et al*., 1998, 2002; Fischer *et al*., 2002; Valsala and Ikeda, 2007).

The right panels of Fig. 1 show the anomalies in the year 2000. The anomalies shown here are based on a 58-year seasonal average. The strengths of the anomalies may explain the departure of the pathways shown here from those appear in a climatological data. It can be seen that the anomalies have mixed (i.e. positive and negative) responses near the western coast. Area-averaged responses of the anomalies along the Somali coast show a relatively stronger upwelling by roughly 9% compared to the climatological values. On the other hand, the Arabian coast anomalies are not so far from the climatological values.

3. Pathways of the Upwelled Water

3.1 Western Arabian Sea upwelling

The upwelled water can be tracked using active non-conservative tracers such as sea surface temperature, salinity or chlorophyll concentrations. However, the temperature and salinity adjust to the surface forcing rather quickly and cannot indicate the state of a particular water mass after the upwelling. The chlorophyll is a good tracker for upwelled water but they are not conservative in a sense that the biological consumption may mask a particular water type. On the other hand, using these parameters we can validate the model passive tracers in the immediate vicinity of the upwelling regions. This validation can check the clarity of the method of tracing the water masses using passive tracers in the numerical models.

Figure 2 shows the surface tracer concentration during the first summer monsoon season of the simulation period. The formulation of the advection-diffusion equation in the offline model is in flux form and thus the tracers are additive in nature. The overall evolution of the tracer can be obtained by summing up individual tracers. The two tracers (ST and AT) are summed together and the solutions are compared with the SST observations in Fig. 2. SST is derived from the TMI/TRMM satellite observations (Wentz, 1997). The SST and the tracer patterns are roughly complementary to each other. This indicates an association of low SST with upwelled waters as well as higher tracer concentrations.

During the month of June the regions of lowest SST is located at the northern flank of GW and circulated anticyclonically, forming a wedge-shaped cold water filament. The corresponding tracer concentration shows the pathway of this upwelled water as a circulation surrounding GW. The Arabian coast has lowest SST centered at 19°N. The tracer shows a maximum Arabian coastal upwelling at this location.

During the month of July, the cold wedge at the northern flank of GW is further extended to the south rotating anticyclonically. The tracers show a detailed structure of this circulation pathway. Another cold wedge is also visible in the northern flank of SE. The corresponding tracer concentrations show that the upwelled water rotates anticyclonically surrounding SE and forms a cold filament there. The upwelling along the coastal Arabia also

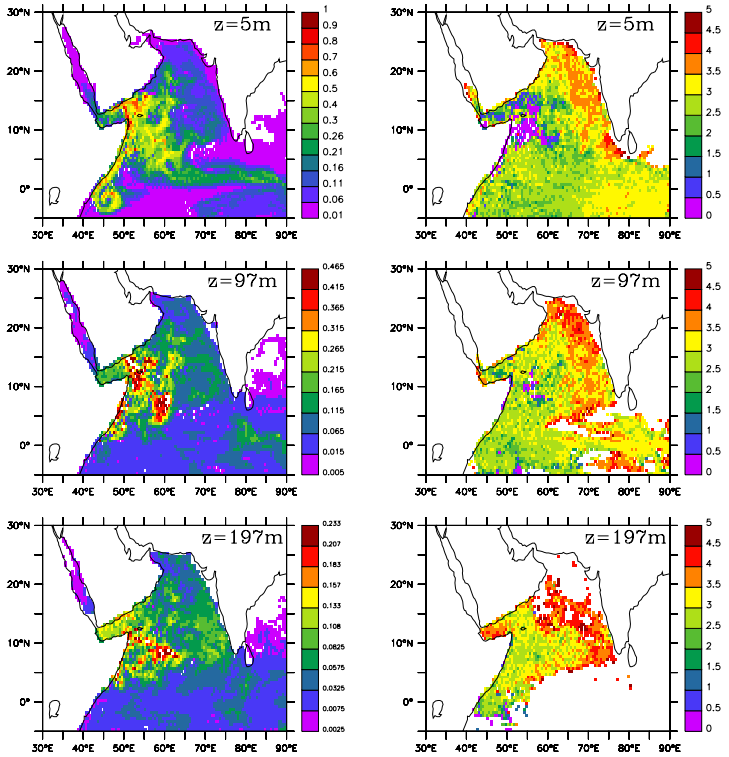

Fig. 3. Left panels: The Somali tracer concentration at the fifth year of the simulation at the 5 m, 97 m and 197 m levels. The scale ranges of z = 57 m, 97 m are half, quarter of the scale range of z = 5 m, respectively. Right panels: The time scale of advancement of a domain average concentration contour front for z = 5 m, 97 m and 197 m. The unit is in years.

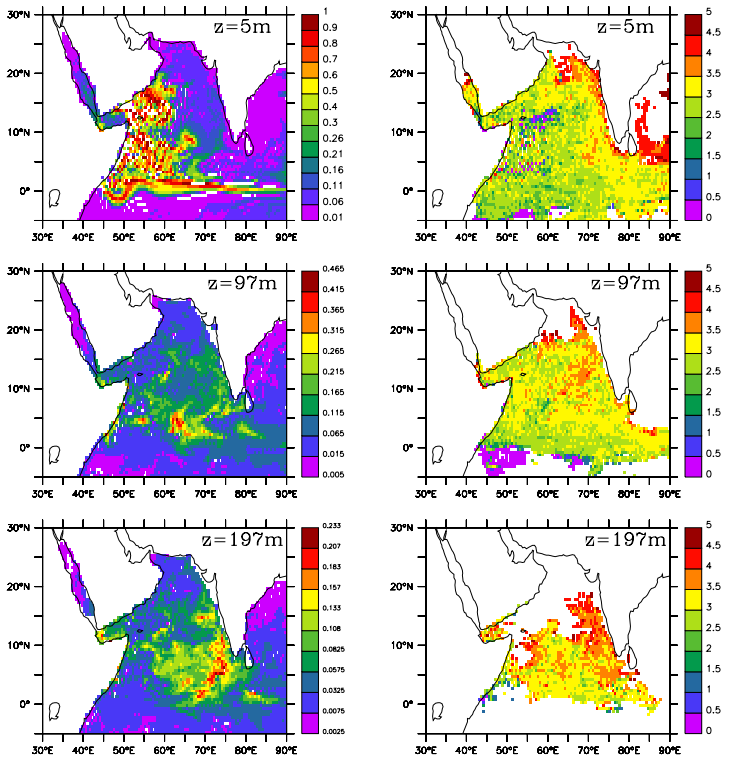

Fig. 4. Same as Fig. 3 but for no seasonal surface vertical mixing.

intensifies during this time and cold filaments are visible along the coast. The tracer shows high concentration along the coastal Arabia for the month of July.

During the month of August, in which the summer monsoon is at its full strength, the upwelled water is spread across and reached far away from the coast. The cold filaments are still discernible in the SST and the filaments that are more obvious are co-located in the tracer maps. It is interesting to note that half of the Arabian Sea basin is occupied with low SST water, which has partially been upwelled through the coastal areas. The spreading of this upwelled water in the tracer maps confirms this. It is tempting to conclude that the low SST region found in the western half of the Arabian Sea is due to the spreading of cold upwelled water. However, this is not the only cause of low SST there. The evaporative cooling due to strong southwesterly winds also causes a cold western Arabian Sea. Vecchi *et al*. (2004) and Seo *et al*. (2008) identified coherent structures of air-sea interaction and oceanic eddies in this region.

3.2 Pathways of the Somali coast upwelled water

Upwelled water can be tracked for a season by monitoring SST as described above. However, strong air-sea interactions and the annual cycle of solar excursions makes tracking of the watermass over a long period from SST difficult. Here, we can rely on tracers to identify watermass spreading pathways.

Figure 3 shows the concentrations of ST (left panel) at the end of the fifth year of the integration. The unit is in number of tracers per unit volume. The solutions are shown for three depth levels and they are 5, 97 and 197 m. The scale range for the 57, 97 m levels are exactly the half, quarter of that of the 5 m plot, respectively.

The mean pathways during the first five years resolved by the tracer show that the Somali upwelled water circulate anticyclonically in GW and SE regions. They are transported to the east across the Indian Ocean and then to the south by the cross-equatorial transport in the eastern Indian Ocean. This pathway is further similar to the one derived from the particles and tracers that cross the equator northward via Somali current (Jensen, 2003; Valsala and Ikeda, 2007). ST were high in concentration in the vicinity of GW and SE. A part of ST is also seen as it advects southward along the Somali coast and recirculates anticyclonically (in the southern part of the equator). This pathway is resolved by the southward winter monsoon circulation nearby the Somali coast and recirculations along the western boundary of the equatorial Indian Ocean.

The concentration of ST at a depth of 97-m suggests that after the upwelling at the Somali coast a part of the water can be transported downward by detrainment and vertical mixing. The maximum concentration is about 50% of that existing in the surface level and is seen in the far eastern flank of GW and some portions to the south of Socotra. In Fig. 1 it can be seen that the vertical velocity is upward in the Somali coast region and on the northern flank of GW, while it is downward in the far eastern part of GW. Thus, there are distinct regions of upwelling and downwelling that exist in the vicinity of GW and SE and cause the downward motion of the upwelled water immediately after the upwelling. This is consistent with the findings of Song *et al*. (2004) who showed that the Lagrangian particles that cross the equator via Somali currents upwell at the Somali coast and then move upward and downward off the coast.

In addition to detrainment by convection processes, the vertical mixing also contributes to the concentration at the 97-m level. Concentration at the 197-m depth (Fig. 3) also indicates that the tracer can reach even to this deeper level in the eastern part of GW and SE and is about 25% of that at the surface. A visible difference between the ST concentration at the 5 m level from those at the 97 m and 197 m levels is that the ST at the surface has a distinct eastward traveling component across the Indian Ocean, whereas in the subsurface ST is spread more into the Arabian Sea than traveling across the Indian Ocean. A noticeable amount of ST can be found along the western coast of India at depths of 97 m and 197 m.

The right panel of Fig. 3 shows the time evolution of a particular valued tracer contour front over the five year period. This can represent the time scale of the upwelled water to reach a given location after its upwelling. This plot is created as follows. An average concentration of ST is found in an ocean region bounded between 35°E–95°E, 5°S–30°N, and 0–47 m. Then a concentration contour front of this average value is searched for. The evolution of that contour front is converted into a corresponding time. It is noted that the box average concentration used to search the contour front increases with time because of the accumulation of tracer in the model domain.

The time scale of ST spreading is given in years in the right panel of Fig. 3. As expected, the recently upwelled water (hereafter referred to as “young water”) is found in the vicinity of the upwelling region and in the GW and SE region. It takes only a few months for this water to get transported from this region to the rest of the Arabian Sea. Water masses with ages about 2~2.5 years can be found in the southeastern part of the domain. There exists a distinct boundary between relatively young water and old water in the northwest to southeast direction through the center of the Arabian Sea. This shows that after the upwelling the water is circulated anticyclonically and traveled to the east across the Indian Ocean. It takes nearly two years for the tracer to reach the eastern Indian Ocean with a concentration equal to the average concentration found in the box being considered here.

The southeastern part of the domain has upwelled water with ages over 3 years. This is the cross-equatorial transport of the water in the eastern Indian Ocean (Jensen, 2003). The oldest water at the surface level is found along the west coast of India. This is a zone where the Somali upwelled water finally reaches in the domain in five years. This is mainly because the majority of the Somali water recirculates anticyclonically immediately after upwelling, and advects to the east without entering to the western Indian coastal region. A minor portion slowly migrates via advection and lateral diffusion and reaches the western Indian coastal region in 4 years or more.

The age of Somali upwelled waters at the 97 m depth shows a relatively similar picture as that at the 5 m. The only difference is that the eastward spreading is relatively delayed in the subsurface layer obviously because of the weaker subsurface currents. The age of upwelled water at the 197 m shows that advection at this depth is even slower and the upwelled waters of 5 years old are still in the central Arabian Sea.

It was mentioned earlier that the presence of ST at a depth of 97 m and 197 m is a consequence of vertical transport and seasonally-driven surface vertical mixing. In order to isolate the effect of vertical advection from the mixing we carried out a separate ST experiment with no seasonal surface vertical mixing included. We note here that the offline SODA data we used in this isolation experiment is same as the one in the previous experiment. It combines the effect of both the vertical mixing and vertical transport. However, the vertical mixing is suppressed only in the passive tracer evolution. The experiment shows that even though the offline input used is the same for both cases, there are significant differences in tracer evolution between the cases with and without surface vertical mixing. This is indeed a consequence of the fact that surface seasonal vertical mixing fluxes are larger in magnitude than the advective vertical transport. The resulting solutions are shown in Fig. 4.

An obvious difference between the cases with and without surface vertical mixing is that the surface concentration of ST is lower in the former than in the latter. In the non-mixing case, ST tends to reside in the surface level, being recirculated and advected to the east across the Indian Ocean. This is quite an expected pathway in the absence of vertical mixing.

The ST concentrations at the 97 m and 197 m levels in the non-mixing case are significantly different. A high concentration of ST is found in a region between 60°E–80°E, 0–10°N in the subsurface layer. This is not seen in the vertical mixing case. Thus, the vertical mixing has an important role in the resultant pathway of the upwelled water from the Somali coast. A major difference is also found in the GW and SE regions at these depths. The ST concentrations in the non-mixing case in these regions

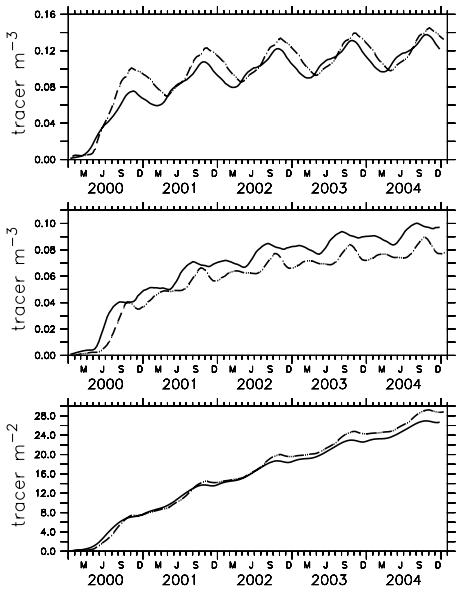

Fig. 5. The average tracer concentration in the 0–47 m (upper panel) and 47–97 m (middle panel) layers in an oceanic region over the Indian Ocean (35°E–95°E, 5°S–30°N). The solid and dashed lines show the results of the control tracer simulation and the zero surface vertical mixing run, respectively. The bottom panel presents the depth integrated concentration obtained through the control tracer run (solid line) and zero surface vertical mixing run (dashed line).

are relatively negligible compared to the case with vertical mixing. Thus, not only the detrainment but also the vertical mixing due to the strong surface momentum forcing by the monsoon winds and the sheared baroclinic currents related to the eddies in the GW and SE regions cause the upwelled Somali water to mix with subsurface water at the level of 100 m.

The relative difference in ages of water between mixing and non-mixing cases is also noticeable in Fig. 4. In the non-mixing case, the Somali upwelled water was brought to the Bay of Bengal by the end of 5 years, whereas in the mixing case the water is slow in spreading to the east of the Indian Ocean because of partial downward dissipation. Thus, the vertical mixing not only influences the pattern of the pathway but also the time scale of the water transport. The age difference between the mixing and non-mixing cases is also visible at the 97 m and 197 m depths.

Figure 5 shows the average concentration of ST in a region bounded between 35°E–95°E, 5°S–30°N at the surface (0–47 m; upper panel) and subsurface (47–97 m; middle panel) levels from the mixing (full line) and non-mixing (dash line) cases. It can be seen that ST is more accumulated in the surface layer in the non-mixing case than in the mixing case. Obviously, this is because the

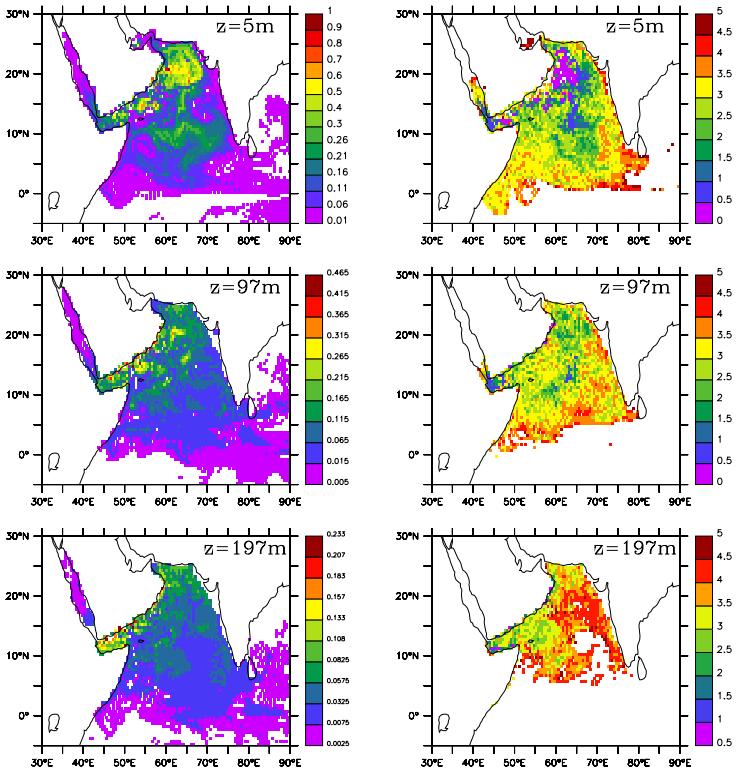

Fig. 6. Same as Fig. 3 but for the Arabian coastal tracer.

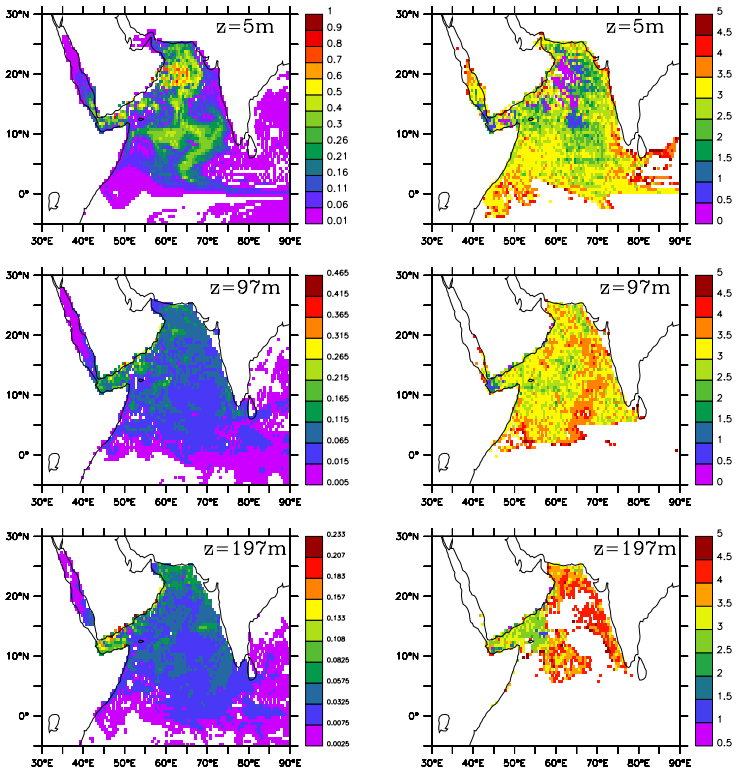

Fig. 7. Same as Fig. 4 but for Arabian coastal tracer.

mixing dissipates the tracer concentration downward. In the subsurface layer, the concentration of ST is about 25% higher in the mixing case than in the non-mixing case. Thus, the vertical mixing in the surface causes 25% of the upwelled Somali water to mix with the water in the subsurface layer. The bottom panel of Fig. 5 shows the depth-integrated concentrations for mixing and non-mixing cases. As expected, both the cases showed similar values because the net tracer quantity injected to the model domain is the same in both experiments. A small difference between the two is due to spreading of ST to outside the boundary of the considered region.

3.3 Pathways of the Arabian coast upwelled water

In this section, the Arabian coastal upwelled water pathways are described. The left panels of Fig. 6 show the concentration of AT at the end of the fifth year calculated at the same three depths as we used in the previous section. At the 5 m level AT is found to be migrating to the northern Arabian Sea, and circulating anticyclonically. It then advects to the south and spread out at 10°N in the central Arabian Sea. It is interesting to note that negligible amount of AT is present in the GW and SE regions. Thus the Arabian coastal upwelled water shows an entirely different pathway from that of the Somali upwelled water. This is an interesting point we noticed in our study. Each upwelling water appears to have entirely different pathways in the Arabian Sea.

At the depths of 97 m and 197 m, AT is found to be spread out within the Arabian Sea. AT at higher concentrations can still be seen along the coastal Arabia and northern Arabian Sea at these depths. The concentration is particularly high in the Gulf of Aden at the 197 m level.

The age of AT at these three depths is shown on the right panels of Fig. 6. An important inference drawn from the ages of ST and AT is that, AT spreads relatively slower than ST. The relatively young AT can be found in the northern Arabian coast which shows that immediately after upwelling the Arabian coast water reaches that region. Along the spreading pathway the younger AT can be found. An interesting point is that along the western coast of India the age of AT is 3 years and more, while that in the central Arabian Sea is less than one year. The major reason for the longer stay of AT along the western coast of India is the northward flowing coastal current that opposes the southward spreading of AT. At the depths of 97 m and 197 m older water is seen. The age at 197 m level is of particular interest since AT older than 5 years is found in the northern part of the Arabian Sea at this depth.

Figure 7 summarizes the pathways of AT in the absence of seasonal vertical mixing. It can be seen that unlike the case of Somali upwelled water, the Arabian coastal water pathways are less influenced by seasonal vertical

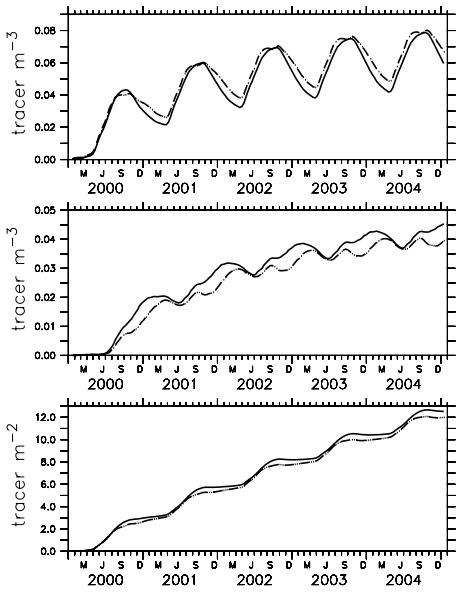

Fig. 8. Same as Fig. 5 but for the Arabian coastal tracer.

mixing. This is clearly seen in the top panels of Figs. 6 and 7 (z = 5 m). The concentrations and age patterns in both figures are nearly identical, although slight differences in total concentrations are found. This is equally true at the 97 m and 197 m levels. Thus, compared to the Somali coastal upwelled water, the pathway of Arabian coast upwelled water is not affected by the vertical mixing.

The age of AT in the non-mixing case is also not so different from that of the mixing case. In contrast to the ST non-mixing case, the relative spreading time of AT in the non-mixing case is not different from that of the mixing case. This is an obvious consequence of the fact that the vertical mixing is found insignificant in determining the AT pathways in contrast to the ST pathways.

Figure 8 summarizes total concentrations of AT in the 0–47 m layer (upper panel) and the 47–97 m layer (lower panel) analyzed in the same oceanic region considered in the ST case. It can be seen in the figure that the average concentration of AT in the two layers are not so different from each other. Hence, the seasonal surface vertical mixing may not be so significant in the pathways of Arabian coastal upwelled water. The average concentration in the 47–97 m layer shows a maximum difference of less than 10%. Thus a 10% of Arabian coastal upwelled water is mixed with the subsurface water after the upwelling. This is smaller than the corresponding 25% in the case of Somali coast upwelled water. The depth integrated concentration for non-mixing case and mixing case are also shown in the bottom panel of Fig. 8 and they are close as expected.

The important results that come out of resolving the pathways of Somali and Arabian coastal upwelled water are that (a) Somali and Arabian coastal waters take entirely different pathways in the Arabian Sea after upwelling; (b) the Somali water travels faster than the Arabian waters; (c) the seasonal surface mixing combines nearly 25% of Somali upwelled water with the subsurface water in addition to the major component of vertical detrainment and has a major influence on the resultant pathway; (d) the Arabian coastal upwelled water pathway is weakly influenced by vertical mixing. The reason why the vertical mixing is an important factor for ST and not for AT is because the location of the ST origin overlaps with the intense current regions of GW and SE where surface mixing is driven not only by intense momentum forcing of the southwesterly Somali winds but also by the shear instability in the water column due to intense eddies. In contrast, the Arabian coastal upwelling waters are not mixed so intensively as Somali upwelled water and thus is mainly transported via advection.

3.4 Relative occupancy of the upwelled water

The complementary patterns of ST and AT pathways (see Figs. 3 and 6) give us a clue to the presence of Somali and Arabian coastal upwelled water in the northern Indian Ocean. For example, the majority of ST, at any instant, occupies a region across the north equatorial Indian Ocean while the concentration of simultaneously-upwelled AT is minor there. This means that ST spreads across the Indian Ocean faster than AT. While in the northern part of the Arabian Sea the situation is opposite, i.e., a major occupation of AT rather than simultaneously upwelled ST.

A more quantitative measure of relative occupancy of simultaneously upwelled waters from the Somali and Arabian coast at any location in the northern Indian Ocean is possible using the tracer analysis, provided that the patterns presented here are consistent for all the years. The consistency of the patterns can be assured by considering the fact that the tracer injection was the same for all the years of the run and the circulation was kept the same as that of the year 2000. This way, the spreading pathways of tracer for any period presented here can be the same for other years of the run as well.

A relative contribution by each of the simultaneously-upwelled water in the northern Indian Ocean is found by calculating a ratio of concentrations of ST and AT to the sum of both the tracers. Figure 9 shows the relative occupancy of water that upwelled simultaneously from the two coastal regions of the western Arabian Sea. As expected from the complementary patterns of ST and AT in Figs. 3 and 6, the percentage occupancy of the Somali and Arabian coast upwelled water in the northern Indian Ocean has distinct patterns. The advection of each of these

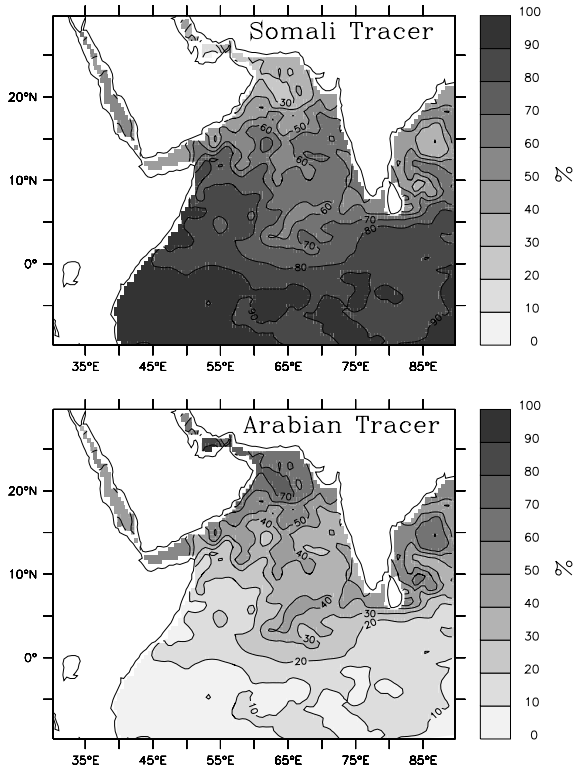

Fig. 9. Percentage concentration of Somali (upper panel) and Arabian (lower panel) coastal upwelled tracers. The figure shows ratios of depth integrated individual tracer to the sum of total tracers. The results shown are at the fifth year of the simulation. A complementary pattern in the residence of the Somali and the Arabian coastal tracer, is visible.

upwelled water and their mixing processes are different, and therefore their pathways are not uniform. The tracer analysis gives a clue on how the upwelled water spreads and how different the pathways are from one another.

The ST are predominantly seen in the southern half of the Arabian Sea, while AT are concentrated in the northern part. The percentage concentration of ST in the northern Arabian Sea is only 30% and the remaining 70% of the total upwelled water there comes from AT. It should be noted that these percentages represent the amount of each upwelled water compared to the total upwelling found in the western coast of Arabian Sea (not the percentage of individual water). At any given time, the upwelled water throughout the northern part of the near-equatorial region in the Indian Ocean mainly originated from the Somali coast. The percentage contribution of ST is above 70% to the total across the Indian Ocean while that of AT is below 30%.

In the northern part of the Arabian Sea, the upwelled water is mainly supplied from the Arabian coast. The contribution from AT is above 70% there, whereas that from

ST is less than 30%. The central Arabian Sea is a region where the equal contributions from both AT and ST are found. This boundary extend from east to west, indicating that the Somali coast upwelled water can intrude into the central Arabian Sea and the Arabian coast upwelled water moves into the northern Arabian Sea, and both of these waters mix at the central Arabian Sea.

Seasonal changes in the circulation have noticeable roles in distributing ST and AT in the Arabian Sea. The dominance of GW and SE during the summer monsoon causes a change in the spreading pathways of ST compared to the winter monsoon. During the summer monsoon, AT recedes further to the northern Arabian Sea. AT are relatively absent in the GW and SE regions during this period.

The pathway sequence of the Somali upwelled water is as follows: upwelling at the Somali coast, circulating anticyclonically around GW and SE, mixing vertically, being advected to the eastern Indian Ocean, and crossing the equator from north at the eastern boundary. A part of the Somali upwelled water intrudes into the northern part of the Arabian Sea. The pathway sequence of the Arabian coastal upwelled water is as follows: upwelling at the Arabian coast, intruding into the northern Arabian Sea, being advected southward through the central Arabian Sea and then to the eastern Indian Ocean and undergoing similar pathways as Somali upwelled water there.

4. Discussion

The occupancy of upwelled water in the northern Indian Ocean that come from various upwelling regions in the western Arabian Sea indicates that the water's upwelling origin and seasonality play significant roles in distributing the upwelled water in distinct spatial patterns. This implies that differences in water properties caused by the upwelling will also have this spatial dependency according to its spreading.

More than 70% of Somali upwelled water circulates around the GW and SE anticyclonically, recedes to the southern Arabian Sea, and is advected to the eastern Indian Ocean through the summer monsoon current. This is similar to the annual mean pathway of the upwelling water from the Somali region that was resolved in the study of Valsala and Ikeda (2007). Thus, it turns out that the seasonality may cause as much as 30% of the upwelled water from the Somali coast to spread to the northern Arabian Sea.

The age of the upwelled water in the surface layer of the Indian Ocean is relatively shorter. After upwelling they are carried to the south through the annual-mean Ekman transport. It takes five years for the Somali upwelled water to be transported to the eastern Indian Ocean and eventually cross the equator. There, they are either routed to the northern Indian Ocean via western boundary (Somali) currents or subducted into the southern tropical Indian Ocean (Valsala and Ikeda, 2007). However, this returning of the tracer does not affect the estimation of the relative concentration presented here. The re-entry of those tracers, which are transported to the south via cross-equatorial transport, takes much longer. Thus, the analysis based on the first five years of tracer integration is not affected by the revisit of the tracer through the Somali current.

4.1 Uncertainties

A source of uncertainty in the present analysis may be the assumption of year 2000 data as the climatology basis; there may be an interannual signal and thus the pathways shown here may have slight differences from the climatology pathways (Krishnan *et al*., 2000). The Findlater Jet (a prime cause of the summer monsoon upwelling in the western Arabian Sea; Findlater, 1969) in 2000 was relatively stronger (figure not shown). This resulted in a Somali upwelling relatively stronger roughly by 9% than the climatology (cf. Fig. 1; bottom-right panel). Therefore, the estimated pathways of ST should be viewed with this order of uncertainty in their strength. It may also be worth mentioning that a faster spreading of upwelled water from the Arabian Sea appears to take place during ENSO and the Indian Ocean Dipole (IOD) years, while the dispersion is slower during La Niña years (Jensen, 2007).

The usage of monthly fields may suppress the high frequency variability in pathways (see Subsection 2.2). Moreover, the transition of offline data at the end of each month to the following month as well as at the end of each year to the following year may cause slight numerical discontinuity in the integration. However, such discrepancies have qualitatively little impact on the results over the limited years presented here. This is confirmed by Fig. 2 that shows that the upwelling cold filaments are relatively captured by the tracers. It should be noted that a sensitivity study on the vertical mixing of various strengths was not performed here. However, from the percentage of mixing in the ST case (25%), one might expect a range to this value according to the variabilities of vertical mixing. A separate study is necessary for investigating the interannual variability in the vertical mixing and circulation as well as the subsequent variability in the pathways.

Finally, the pathways shown here are the numerical solution derived in an OGCM. These model predicted pathways were not verified by any real tracers: in fact, it is difficult to establish with available observations. It is noteworthy that Grumet *et al*. (2002) used coral radiocarbon observations and were able to find its southward transport across the equator. However, our numerical trac-

ers were verified using satellite derived SST and the pathways were found to be reliable. In addition, the model circulations were also verified using satellite observations. Thus it can be assumed that within the accuracy of circulation and transport modeling, the pathways derived here using numerical tracers are reasonable.

5. Summary

A re-analysis OGCM data set was used in an offline-mode to evolve a passive tracer and was used to find pathways of upwelled water from the western coast of the Arabian Sea over a five year period. The tracers were tracked separately to study waters upwelled from the Somali and Arabian coastal regions. The Somali upwelled water recirculates anticyclonically in the GW and SE regions and is advected eastward across the Indian Ocean along the north of the equator. The seasonal circulation and vertical mixing are found to be significant controls on the resultant pathways of the Somali upwelled water. 25% of the Somali upwelled water is dissipated to the subsurface by vertical mixing. The water upwelled from the coast of Arabia occupies the northern part of the Arabian Sea. In contrast to the case of Somali waters, the pathways of upwelled water from the Arabian coast were unaffected by the seasonal vertical mixing. The seasonal reversal of circulation and eddy dominance during southwest monsoon caused the Somali water to spread over the Indian Ocean faster than the Arabian coast upwelled water.

This work described the occupancy of each upwelling water from various coastal regions of western Arabian Sea in the northern Indian Ocean. Considering the impact of the Arabian Sea coastal upwelling on the Indian Ocean climate system and monsoon, it is desirable to see the fate and variability of these upwelling water routes. Izumo *et al*. (2008) noticed that a weaker-than-usual coastal upwelling in the western Arabian Sea led to an increased precipitation in the western Indian land region because of an enhanced evaporative moisture transport. It was found out in this study that the seasonal vertical mixing caused a 25% of upwelled water from the Somali coast to mix with the subsurface water, thereby being able to modify the SST, which is consistent with the findings of Montegut *et al*. (2007) as well. In considering these factors, our study helps to identify the regions where the upwelling waters have immediate influences on the surface ocean water properties.

The biological production in the western Arabian Sea peaks during the upwelling season because of the availability of nutrients from the subsurface. However, Wiggert *et al*. (2006) noticed that the western side of the Arabian Sea was prone to seasonal iron limitation despite its constant dust supply from desert regions. Adding to this, our study suggests that the vertical mixing of upwelled water in the Somali coastal region may also contribute to the dissipation of the newly upwelled surface nutrients. This may shield the upwelled nutrients from the reach of Photosynthetically Active Radiation (PAR) and may result in a reduced biological production. This sheds light on the fact that seasonal vertical mixing not only influences the upwelling water trajectories (and the nutrient trajectories partially as well) but also may cause variabilities in biological production. Further studies are required to investigate the interannual pathway of upwelling waters from the western coast of Arabian Sea and the ecosystem.

Acknowledgements

The author acknowledges the financial support from the GOSAT project operating at the National Institute for Environmental Studies (NIES), Tsukuba, Japan and the Japan Society for the Promotion of Science (JSPS) in order to carry out this study. Model simulations were carried out in the supercomputer facility at NIES. The author thanks Drs. T. Jensen, S. Godfrey and one anonymous reviewer for their valuable comments on a previous version of this manuscript and two other anonymous reviewers for their encouraging feedback on the present version of the manuscript. The SODA data used in this study were obtained from http://dsrs.s.atmos.umd.edu/DATA/. Mr. Hiroshi Takagi is acknowledged for correcting the English. Ferret software (NOAA/PMEL) was used for plotting.

References

Carton, J. A. and B. S. Giese (2008): A reanalysis of ocean climate using Simple Ocean Data Assimilation (SODA). *Mon. Wea. Rev.*, **136**, 2999–3017.

Conkright, M. E., R. A. Locamini, H. E. Gracia, T. D. O'Brien, T. P. Boyer, C. Stephens and J. J. Antonov (2001): *World Ocean Atlas 2001: Objective Analyses, Data Statistics and Figures, CD-ROM Documentation*. National Oceanographic Data Center, M.D., 17 pp.

Findlater, J. A. (1969): A major low level air current over the Indian Ocean during the northern summer. *Quart. J. Roy. Meteor. Soc.*, **95**, 280–362.

Fischer, A. S., R. A. Weller, D. L. Rudnick, C. C. Eriksen, C. M. Lee and K. H. Brink (2002): Mesoscale eddies, coastal upwelling and the upper-ocean heat budget in the Arabian Sea. *Deep-Sea Res.*, **49**, 2231–2264.

Ganachaud, A. and C. Wunsch (2000): Improved estimate of global ocean circulation, heat transport and mixing from hydrographic data. *Nature*, **408**, 453–456.

Gent, P. R. and J. C. McWilliams (1990): Isopycnal mixing in ocean circulation models. *J. Phys. Oceanogr.*, **20**, 150–155.

Godfrey, J. S., R. Hu, A. Schiller and R. Fiedler (2007): Explorations of the annual mean heat budget of the Tropical Indian Ocean. Part I: Studies with an idealized model. *J. Climate*, **20**, 3210–3228.

Grumet, N. S., T. P. Guilderson and R. B. Dunbar (2002): Me-

ridional transport in the Indian Ocean trace by coral radiocarbon. *J. Mar. Res.*, **60**, 725–742.

Izumo, T., C. B. Montegut, J. J. Luo, S. K. Behera, S. Masson and T. Yamagata (2008): The role of the western Arabian Sea upwelling in the Indian monsoon rainfall variability. *J. Climate*, **21**, 5603–5623.

Jensen, T. G. (1991): Modeling of Somali Undercurrents in the Somali Current System. *J. Geophys. Res.*, **96**, 12151–12167.

Jensen, T. G. (2003): Cross-equatorial pathways of salt and tracers from the northern Indian Ocean: Modelling results. *Deep-Sea Res.*, **50**, 2111–2127.

Jensen, T. G. (2007): Wind-driven response of the northern Indian Ocean to climate extremes. *J. Climate*, **20**, 2978–2992.

Kindle, J. C. and J. D. Thompson (1989): The 26- and 50-day oscillations in the western Indian Ocean: Model results. *J. Geophys. Res.*, **94**, 4721–4736.

Krishnan, R. C., C. Zhang and M. Sugi (2000): Dynamics of Breaks in the Indian Summer Monsoon. *J. Atmos. Sci.*, **57**, 1345–1372.

Large, W. G., J. C. McWilliams and S. C. Doney (1994): Ocean vertical mixing: A review and a model with a nonlocal boundary layer parameterization. *Rev. Geophys.*, **32**, 363–403.

Miyama, T., J. P. McCreary, T. G. Jensen, J. Loschnigg, S. Godfrey and A. Ishida (2003): Structure and dynamics of the Indian-Ocean cross-equatorial cell. *Deep-Sea Res.*, **50**, 2023–2047.

Montegut, D. B., J. Vialard, S. S. C. Shenoi, D. Shankar, F. Durand, C. Ethe and G. Madec (2007): Simulated seasonal and interannual variability of the mixed layer heat budget in the northern Indian Ocean. *J. Climate*, **20**, 3249–3268.

Redi, M. (1982): Oceanic isopycnal mixing by coordinate rotation. *J. Phys. Oceanogr.*, **12**, 1154–1158.

Schott, F. A. and J. P. McCreary (2001): The monsoon circulation of the Indian Ocean. *Prog. Oceanogr.*, **51**, 1–123.

Schott, F. A., J. C. Shallow and M. Fieux (1990): The Somali Current at the equator: annual cycle of currents and transports in the upper 1000 m and connection to neighboring latitudes. *Deep-Sea Res.*, **37**, 1825–1848.

Schott, F. A., J. Fischer, U. Garternicht and D. Quadfasel (1997): Summer monsoon response of the northern Somali Current, 1995. *Geophys. Res. Lett.*, **24**, 2565–2568.

Schott, F. A., M. Dengler and R. Schoenefeldt (2002): The shallow overturning circulation of the Indian Ocean. *Prog. Oceanogr.*, **53**, 57–103.

Sengupta, D., R. Senan, V. S. N. Murty and V. Fernando (2004): A biweekly mode in the equatorial Indian Ocean. *J. Geophys. Res.*, **109**, doi:10.1029/2004JC002329.

Seo, H., R. Murtugudde, M. Jochum and A. Miller (2008): Modeling of mesoscale coupled ocean-atmosphere interaction and its feedback to ocean in the western Arabian Sea. *J. Climate*, **25**, 120–131.

Shankar, D. and S. R. Shetye (1997): On the dynamics of the Lakshadweep high and low in the southeastern Arabian Sea. *J. Geophys. Res.*, **102**, 12551–12562.

Sharada, M. K., P. S. Swathi, K. S. Yajnik and C. K. Devasena (2008): Role of biology in the air-sea carbon flux in the Bay of Bengal and Arabian Sea. *J. Earth Syst. Sci.*, **117**, 429–447.

Song, Q., A. L. Gordon and M. Visbeck (2004): Spreading of Indonesian Throughflow in the Indian Ocean. *J. Phys. Oceanogr.*, **34**, 772–792.

Valsala, K. V. and M. Ikeda (2007): Pathways and effects of the Indonesian Throughflow water in the Indian Ocean using Particle trajectory and Tracers in an OGCM. *J. Climate*, **20**, 2994–3017.

Valsala, K. V., S. Maksyutov and M. Ikeda (2008): Design and validation of an offline oceanic tracer transport model for a carbon cycle study. *J. Climate*, **21**, 2752–2769.

Vecchi, G. A., S.-P. Xie and A. Fischer (2004): Ocean–Atmosphere covariability in the western Arabian Sea. *J. Climate*, **17**, 1213–1224.

Weller, R. A., M. F. Baumgartner, S. A. Josey, A. S. Fischer and J. C. Kindle (1998): Atmospheric forcing in the Arabian Sea during 1994–1995: observations and comparisons with climatology and models. *Deep-Sea Res.*, **45**, 1961–1999.

Weller, R. A., A. S. Fischer, D. L. Rudnick, C. C. Eriksen, T. D. Dickey and J. Marra (2002): Moored observations of upper-ocean response to the monsoons in the Arabian Sea during 1994–1995. *Deep-Sea Res.*, **49**, 2195–2230.

Wentz, F. J. (1997): A well-calibrated ocean algorithm for special sensor microwave/imager. *J. Geophys. Res.*, **102**, 8703–8718.

Wiggert, J. D., R. G. Murtugudde and J. R. Christian (2006): Annual ecosystem variability in the tropical Indian Ocean results of a coupled bio-physical ocean general circulation model. *Deep-Sea Res.*, **53**, 644–676.